BIOCHEMISTRY
including biophysical chemistry & molecular biology

ARTICLE

pubs.acs.org/biochemistry

Crystal Structure of *Agaricus bisporus* Mushroom Tyrosinase: Identity of the Tetramer Subunits and Interaction with Tropolone

Wangsa T. Ismaya,[†,⊥] Henriëtte J. Rozeboom,[†,⊥] Amrah Weijn,[§] Jurriaan J. Mes,[§] Fabrizia Fusetti,[‡] Harry J. Wichers,[§] and Bauke W. Dijkstra*[,†]

[†]Laboratory of Biophysical Chemistry and [‡]Netherlands Proteomics Centre, University of Groningen, Groningen, The Netherlands
[§]Wageningen University and Research Center, Wageningen, The Netherlands

Supporting Information

ABSTRACT: Tyrosinase catalyzes the conversion of phenolic compounds into their quinone derivatives, which are precursors for the formation of melanin, a ubiquitous pigment in living organisms. Because of its importance for browning reactions in the food industry, the tyrosinase from the mushroom *Agaricus bisporus* has been investigated in depth. In previous studies the tyrosinase enzyme complex was shown to be a H_2L_2 tetramer, but no clues were obtained of the identities of the subunits, their mode of association, and the 3D structure of the complex. Here we unravel this tetramer at the molecular level. Its 2.3 Å resolution crystal structure is the first structure of the full fungal tyrosinase complex. The complex comprises two H subunits of ~392 residues and two L subunits of ~150 residues. The H subunit originates from the *ppo3* gene and has a fold similar to other tyrosinases, but it is ~100 residues larger. The L subunit appeared to be the product of *orf239342* and has a lectin-like fold. The H subunit contains a binuclear copper-binding site in the deoxy-state, in which three histidine residues coordinate each copper ion. The side chains of these histidines have their orientation fixed by hydrogen bonds or, in the case of His85, by a thioether bridge with the side chain of Cys83. The specific tyrosinase inhibitor tropolone forms a pre-Michaelis complex with the enzyme. It binds near the binuclear copper site without directly coordinating the copper ions. The function of the ORF239342 subunits is not known. Carbohydrate binding sites identified in other lectins are not conserved in ORF239342, and the subunits are over 25 Å away from the active site, making a role in activity unlikely. The structures explain how calcium ions stabilize the tetrameric state of the enzyme.

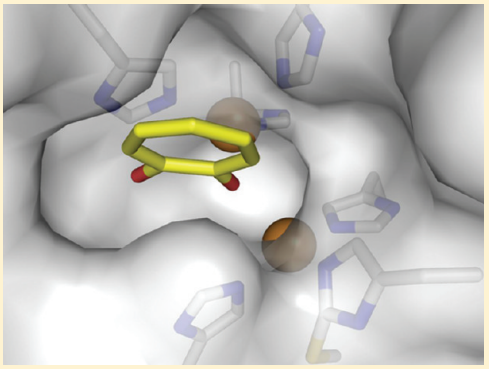

Tyrosinase (EC 1.14.18.1) is a binuclear copper-containing enzyme that catalyzes the conversion of a monophenol (tyrosine) and/or *o*-diphenol (L-DOPA) into its corresponding *o*-quinone derivative (L-DOPA quinone), which is further converted into melanin. Melanin is a pigment that is ubiquitously present in living organisms from all phyla. Since tyrosinase is the key enzyme in the first step of melanin biosynthesis, the enzyme is frequently associated with pigmentation.[1]

So far, four tyrosinase genes of the common button mushroom, *Agaricus bisporus*, have been described. Wichers and coworkers have found two genes that encode two 64 kDa tyrosinases, *ppo1* (Genebank accession number X85113) and *ppo2* (AJ223816).[2] Recently, two other genes encoding a 66 and 68 kDa tyrosinase were reported, *ppo3* (GQ354801) and *ppo4* (GQ354802), respectively.[3]

The enzyme is commonly found as a tetrameric protein with a molecular mass of 120 kDa, composed of two subunits of ~43 kDa (H subunit) and two subunits of ~14 kDa (L subunit).[4] The discovery of an active monomeric 43 kDa tyrosinase isolated from mushroom fruit bodies[5] suggests that the H subunit is tyrosinase. The identity, function, and origin of the L subunit are as yet unknown.[6,7]

Insight into the structure of the mushroom tyrosinases is, so far, based on the structures of a plant catechol oxidase from *Ipomoea batatas* (*Ib*COX)[8] and a bacterial tyrosinase from *Streptomyces castaneoglobisporus* (*Sc*TYR),[9] which have 17−21% sequence identity to ~380 N-terminal residues of the *A. bisporus* tyrosinases. Structures of *Ib*COX showed the various oxidation states of the two copper ions in the active site and the binding mode of the inhibitor phenylthiourea. The *Sc*TYR structure also provided information on the various oxidation states of the copper ions. Although the two structures show a strong structural similarity of tyrosinase and catechol oxidase, the mechanism of the reaction is still under dispute because of disagreement on the substrate-binding mode.[10]

A highly conserved Cys-X-His sequence motif is present in the mushroom tyrosinases.[11] In the fungal *Neurospora crassa* tyrosinase the cysteine and histidine side chains of this motif are connected by a covalent thioether bond,[12] with the histidine residue also functioning as one of the Cu-A coordinating ligands.

Received: March 17, 2011
Revised: May 19, 2011
Published: May 19, 2011

Table 1. Summary of Crystallographic Data Collection and Processing

	native $P2_1$	native-1 $P2_12_12$	tropolone $P2_1$	native-2 $P2_12_12$
beamline	ESRF ID23-2	ESRF ID14-4	ESRF ID23-2	ESRF ID14-4
wavelength (Å)	0.8726	0.9395	0.8726	0.9395
resolution (Å)	50.0−3.0	54.2−2.60	58.0−2.78	61.1−2.30
cell parameters				
a (Å)	104.2	104.0	103.8	104.1
b (Å)	105.0	104.5	104.8	104.5
c (Å)	119.1	108.4	119.4	109.0
β (deg)	110.6	90	110.5	90
R_{merge} [a]	0.16 (0.34)	0.12 (0.45)	0.24 (0.62)	0.12 (0.55)
R_{pim} [a]	0.11 (0.24)	0.07 (0.28)	0.17 (0.44)	0.07 (0.34)
mean $I/\sigma I$	7.3 (2.3)	8.2 (2.3)	3.5 (1.6)	7.7 (2.3)
completeness (%)	88.9 (90.5)	94.8 (81.8)	89.6 (89.7)	99.4 (99.6)
multiplicity	2.8 (2.9)	4.0 (2.7)	2.7 (2.6)	3.7 (3.5)

[a] $R_{merge} = \Sigma_{hkl}\Sigma_i|I_i(hkl) - \langle I(hkl)\rangle|/\Sigma_{hkl}\Sigma_i(hkl)$. $R_{pim} = \Sigma_{hkl}[1/(N-1)]^{1/2}\Sigma_i|I_i(hkl) - \langle I(hkl)\rangle|/\Sigma_{hkl}\Sigma_i(hkl)$. $I_i(hkl)$ is the integrated intensity of a reflection, $\langle I(hkl)\rangle$ is the mean intensity of multiple corresponding symmetry-related reflections, and N is the multiplicity of the given reflections. Values in parentheses are for the highest resolution shell.

Interestingly, this thioether bond is also conserved in mollusc hemocyanin and, with a different sequence motif, in catechol oxidase,[10] which may indicate its importance. However, the thioether bond is absent in the bacterial tyrosinase,[9] and therefore its function remains unclear.

In the present study, we have successfully unraveled the individual components of the tetrameric enzyme complex by a combination of molecular and biochemical analysis. The study started with crystallizing a commercially available tyrosinase enzyme from *A. bisporus* (*Ab*TYR) and elucidation of the structure by means of X-ray crystallography. At the same time a molecular analysis of the recently generated complete *Agaricus bisporus* genome sequence allowed to establish the identity of the H and L subunits of the tyrosinase enzyme complex. Whereas the H subunit originates from a tyrosinase/polyphenoloxidase gene, the L subunit is the product of an unrelated gene with unknown function. A structure of the enzyme complex with the inhibitor tropolone shows that this inhibitor forms a pre-Michaelis complex with deoxytyrosinase. These analyses are of particular interest because commercial mushroom tyrosinase has been employed extensively in various studies for agricultural, industrial, pharmaceutical, and medical purposes. The identification of the complete complex and the binding mode of an inhibitor paves the way for in depth studies of how to regulate the activity of the tyrosinase enzyme.

EXPERIMENTAL PROCEDURES

Protein Purification, Crystallization, and X-ray Data Collection. *A. bisporus* tyrosinase, *Ab*TYR, was purchased from Sigma-Aldrich (St. Louis, MO). Purification and crystallization of the enzyme were done as described elsewhere.[13] Briefly, tyrosinase crystals were obtained at room temperature using the hanging-drop vapor diffusion technique with drops made of a 1:1 mixture of protein solution (~6 mg/mL) in 10 mM HEPES buffer, pH 7.5, and reservoir solution, containing 10% (w/v) PEG4000 in 100 mM sodium acetate buffer, pH 4.6, with 5 mM holmium chloride as additive. After 4−5 days two different crystal forms appeared in the drops, belonging to space groups $P2_12_12$ or $P2_1$. Diffraction data were collected at the European Synchrotron Radiation Facility (ESRF) in Grenoble, France, and processed with the programs XDS[14] or MOSFLM[15] (for details, see Table 1). Scaling and merging of the data sets processed with MOSFLM were done with the program SCALA[16] using the CCP4 interface.[17] The Matthews coefficient, V_M,[18] and self-rotation maps from the program MOLREP[19] suggested that the crystals contained one ($P2_12_12$) or two ($P2_1$) H_2L_2 tetramers of 120 kDa per asymmetric unit. For substrate binding studies diffraction data were collected from a crystal belonging to space group $P2_1$, which had been soaked in reservoir solution containing 5 mM of the inhibitor tropolone (2-hydroxy-2,4,6-cycloheptatrien-1-one) (Table 1).

Peptide Mass Fingerprinting. A tyrosinase crystal was dissolved in water and subjected to SDS-PAGE analysis. After staining with Coomassie Brilliant Blue R25, the bands corresponding to the H and L subunits were excised from the gel. After destaining the gel pieces, the proteins were digested with trypsin and identified by tandem mass spectrometry searching against the UniProtKB/Swiss-Prot protein sequence database.[20] For a detailed description of the procedure see ref 21.

Rapid Amplification of cDNA Ends (RACE). RNA was isolated from 40 mg grinded epidermis tissue of *A. bisporus* (strain Les Miz 36) according to the protocol of total RNA purification from filamentous fungi from Qiagen. DNase treatment of the purified RNA was performed on column with the RNase free DNase set of Qiagen according to the manufacturer's instructions. cDNA synthesis was performed using random primers and SuperScript III RT according to the manufacturer's instructions. The 3′ and 5′ RACE analysis was performed according to the manufacturer's protocol of the GeneRacer kit (Invitrogen) with slight modifications. The GeneRacer 3′ nested primer CGCTACGTAACGGCATGACAGTG and forward L-subunit specific primer GAGGCAACACAGTCCTTGGT were used for the 3′ RACE. For the 5′ RACE the GeneRacer 5′ primer CGACTGGAGCACGAGGACACTGA and reversed L-subunit primer AGTCCAGACAGCACCTCCAC were used. The amplified fragments were separated by 2% agarose gel elecrophoresis, and the fragment with the desired length was extracted from the gel and purified with the QIAquick gel extraction kit from Qiagen according to protocol. The purified

PCR product was cloned into the pCR4-TOPO vector according to the protocol of Invitrogen. Transformation into the competent TOP10 *Escherichia coli* cells was done according to the one shot TOP10 chemically competent *E. coli* protocol from Invitrogen, followed by DNA sequencing of 10 individual clones.

Starting Model and Phasing by Molecular Replacement. On the basis of previous mass spectrometry studies,[6] the PPO2 sequence was selected to search the Protein Data Bank (PDB) for homologous structures, using the FFAS03 server.[22] Four structures were obtained, with highest identity to the N-terminal part of *A. bisporus* PPO2 (ref 2, putative H subunit, ~43 kDa), i.e., *Octopus dofleini* hemocyanin (PDB code 1js8, 17% sequence identity[23]), *Rapana thaliana* hemocyanin (PDB code 1lnl, 17% sequence identity[24]), *I. batata* catechol oxidase (PDB code 1bt1, 17% sequence identity[8]), and *S. castaneoglobisporus* tyrosinase (PDB code 1wx2, 21% sequence identity[9]). No homology model could be obtained for the C-terminal part of PPO2 (putative L subunit, ~14 kDa) because of lack of sequence homology. Using these four structures as templates, homology models were generated with the SCWRL server.[25] Molecular replacement was performed with the program PHASER[26] at 2.6 Å resolution using an ensemble of the four H-subunit homology models, which resulted in a solution with two H-subunit molecules in the $P2_12_12$ asymmetric unit, consistent with the V_M and self-rotation map.

Model Building. The molecular replacement solution was subjected to the automatic model-building program RESOLVE,[27] with noncrystallographic symmetry (NCS) restraints applied. The resulting model covered 580 residues of the two H subunits in the asymmetric unit, with only 180 side chains assigned. It was manually rebuilt with the program COOT[28] against a 2.6 Å NCS-averaged composite omit map, refined with the program REFMAC5,[29] further improved against a new NCS-averaged omit map and resubmitted to RESOLVE. This procedure was iterated until the model did not further improve. Visual inspection of the electron density map obtained from each iterative cycle was used to monitor the progress in the model building. Regularly, the model was transferred to space group $P2_1$ (3.0 Å resolution) to exploit the averaging power of four molecules in the asymmetric unit to extend the main chain of the working model. Moreover, this approach also reduced model bias because of the independency of the data sets. The extended model was then transferred back to space group $P2_12_12$ to continue the iterative model building and refinement procedure. Nevertheless, the refinement stalled at an *R*-factor of 42%, and only an incomplete model was obtained. Next, when a new data set with higher completeness and resolution (2.3 Å) became available, the program ARP/wARP[30] was used to extend the model, also using NCS restraints. Various substitutions and insertions in the H subunit had to be introduced, which were in full agreement with the recently published *A. bisporus* PPO3 sequence.[3] Consequently, the model building of the H subunit was completed using the PPO3 sequence.

The electron density for the L subunit generated by ARP/wARP was not compatible with the amino acid sequence of the C-terminal part of PPO2 or with that of PPO3. Therefore, all residues were set to alanines, and when interpretable side chain density became visible by model building and refinement, changed to amino acids corresponding to the electron density. A BLAST search[31] with the partial amino acid sequence derived from the electron density maps against public sequence databases did not reveal any homologous proteins. However, comparison of this amino acid sequence with sequences derived from open reading frames in the *A. bisporus* genome database gave one clear hit, which allowed completing the model building of the L subunit. The complete genome sequence of *A. bisporus* is still in preparation, and the sequence of the L subunit was kindly provided by the *A. bisporus* genome consortium (Dr. M. Challen, personal communication; http://genome.jgi-psf.org/Agabi_varbisH97_2/Agabi_varbisH97_2.home.html).

Table 2. Summary of Model Refinement

model	native $P2_12_12$	tropolone $P2_1$
R/R_{free} (%)	18.1/23.7	23.6/28.9
resolution (Å)	47.1−2.30	58.0−2.78
HL subunits/ asymmetric unit	2	4
no. of atoms		
protein	8526	17052
	4 Cu, 6 Ho	
ligands	3 diethylene glycol, 1 triethylene glycol	8 Cu, 4 Ho, 4 tropolone
water molecules	390	25
B factors (Å^2)		
main chain H-, L-subunits	31.8, 36.7	55.3, 56.7
Cu^{2+} ions	32.8	47.2
Ho^{3+} ions	44.3	70.2
ligands	40.7	84.5
rms deviations		
bond lengths (Å)	0.010	0.006
dond angles (deg)	1.16	0.95
PDB accession code	2y9w	2y9x

Refinement with REFMAC including TLS optimization[32] finalized the model building, converging to a conventional *R*-factor of 18.1% and an R_{free} of 23.7% (space group $P2_12_12$) and 23.6% and 28.9% (space group $P2_1$) (Table 2). During the refinement the copper−histidine ligand distances were restrained to 2.1 Å. The models were validated with the program MolProbity.[33] A Ramachandran analysis of the HL protomer in space group $P2_12_12$ showed no outliers, with 509 and 14 residues being in the favored and allowed regions, respectively. All ligands, cations, and inhibitor molecules were added after inspection of $F_o - F_c$ difference Fourier maps. A dictionary for the inhibitor tropolone was generated with the PRODRG server,[34] and bond lengths and angles were obtained from the crystal structure of tropolone.[35]

The atomic coordinates and structure factors have been deposited with the PDB with accession codes 2y9w and 2y9x for native and tropolone-bound *A. bisporus* tyrosinase, respectively. The sequence alignment and the structure figures presented in this article were prepared using the programs ALINE,[36] Espript,[37] and PyMol.[38]

RESULTS AND DISCUSSION

Identity of the Crystallized Protein Material. The *A. bisporus* tyrosinase crystals, obtained from the protein material purchased from Sigma-Aldrich, contain both the H and L subunits. Using an ensemble of four structures with only 17−21% sequence homology to PPO2 gave a low-quality molecular replacement solution for the H subunit (see Experimental Procedures). However, at

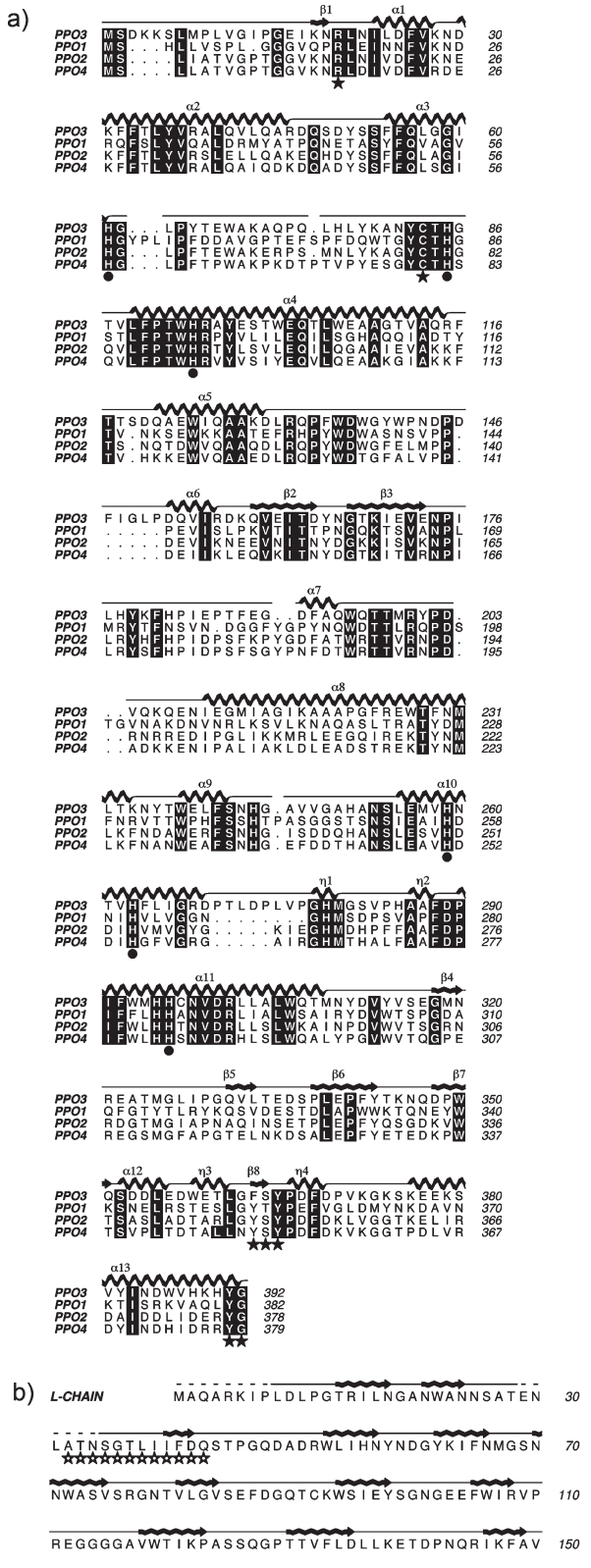

Figure 1. (a) Amino acid sequence alignment of the mushroom tyrosinases PPO3, PPO1, PPO2, and PPO4 (up to PPO3 residue 392) and secondary structure elements of PPO3. The circles indicate the copper-coordinating histidine residues, and the stars show Arg20, Cys83, and the Tyr/Phe-X-Tyr and Tyr-Gly motifs discussed in the text. (b) Amino acid sequence and secondary structure of the L subunit. The stars show the residues previously identified as belonging to the L subunit.[6] The dashes indicate residues not visible in the electron density.

various positions the PPO2 sequence did not match the electron density, and insertions and substitutions had to be introduced. In contrast, the recently reported PPO3 sequence (53.6% identity to PPO2 in the 392 N-terminal residues[3]) fitted the electron density without the need for insertions and deletions. A tandem mass spectrometry analysis of the H subunit isolated from a dissolved crystal confirmed its identity as PPO3 (94% coverage, data not shown). Therefore, the model building of the H subunit was completed with the PPO3 sequence, and henceforth the enzyme will be referred to as PPO3 (Figure 1a).

The identity of the L subunit has so far remained unknown.[6,7,39] It was obvious that the electron density maps did not correspond to any of the C-terminal PPO sequences or the sequences of an *A. bisporus* lectin or putative mannanase suggested previously.[6,7,39] A BLAST[31] search with a partial amino acid sequence of the L subunit derived from the electron density maps against public sequence databases did not reveal any homologous proteins. Making use of the previously identified partial sequence from the L subunit (ATNSGTLIIFDQ[6]), a BLAST search was done in the very recently generated *A. bisporus* genome sequence. This resulted in the identification of a single ORF (protein ID 239342). 3′ and 5′ RACE, cloning and sequence analysis using white button mushroom cap tissue yielded four almost identical full sequences, very likely allelic variations of the same gene. Real-time PCR analysis, using mRNA isolated from fruiting body of white button mushrooms, confirmed expression of the ORF239342 (data not shown). The mature L subunit comprised 150 amino acids (~16.5 kDa, Figure 1b), which showed no significant sequence identity to other proteins. With this sequence the model building of the L subunit was completed. To further confirm the amino acid sequence of the L subunit, protein crystals were dissolved, subjected to SDS-PAGE analysis, and analyzed by tandem mass spectrometry against the *A. bisporus* genome sequence. This analysis confirmed the identity of the crystallized L subunit as the product of *orf239342* (83% coverage; data not shown).

H_2L_2 Tetramer. Mushroom tyrosinase crystallizes with one (space group $P2_12_12$) or two (space group $P2_1$) H_2L_2 tetramers in the asymmetric unit. The tetrameric arrangements in the asymmetric units of the two space groups are different (Supporting Information Figure S1). However, applying the crystallographic 2-fold rotation to a HL dimer in space group $P2_12_12$ generates the same tetrameric arrangement as in space group $P2_1$. In contrast, it is not possible to generate the $P2_12_12$ arrangement by crystallographic symmetry operations of space group $P2_1$. Moreover, the $P2_1$ interaction surface is about 10% larger than that in the asymmetric unit of space group $P2_12_12$ (2980 Å^2 compared to 2680 Å^2 buried surface), suggesting a more stable arrangement. For these reasons we propose that the $P2_1$ tetrameric organization is the one occurring in solution (Figure 2). This tetramer is stabilized by two holmium ions in the H−H interface, each coordinated by the side chains of Asp336, Asp353, and Gln351 from one H subunit and the Asp312 side chain from the other, and by two water molecules. Interestingly, in the $P2_12_12$ crystal form one of the holmium ions occupies two closely related positions, 3.0 Å apart, in a ~70%/30% ratio, indicating that it is not bound very specifically. Holmium is an analogue of calcium, and it was used as an additive in the crystallization experiments. The Ho^{3+} ions possibly diminish the repulsion between the negatively charged residues in the dimer interface, which is in agreement with a previous report that calcium stimulates the association of mushroom tyrosinase into tetramers.[40]

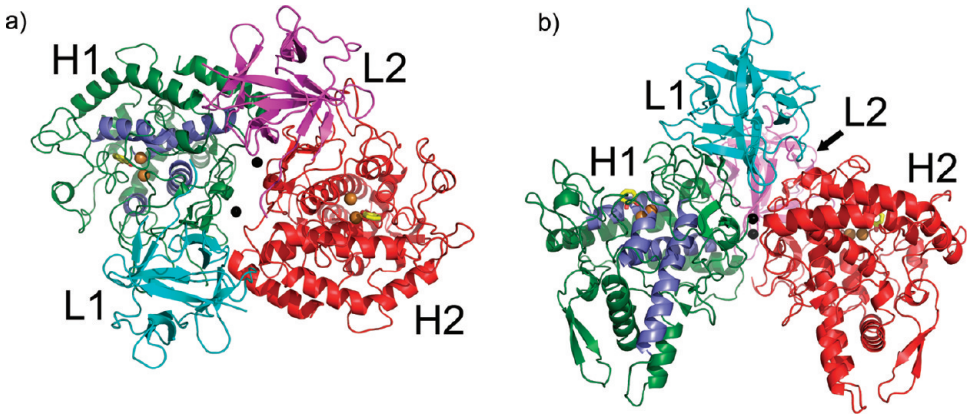

Figure 2. Top (a) and side (b) views of the *A. bisporus* tyrosinase H_2L_2 tetramer structure. H−L dimer interactions are between H1 (green) and L1 (cyan) and H2 (red) and L2 (magenta). The brown and black spheres indicate the copper and holmium ions, respectively, and the yellow sticks the tropolone molecule in the active site. The four α-helices that make up the active site (α3, α4, α10, α11) are marked in blue.

The H−L interface covers an area of ∼800 Å^2; it is stabilized by two salt bridges: His76 (H)−Glu139 (L) and Glu317 (H)−His56 (L) (Figure 3). In addition, hydrogen bonds are present between the peptide nitrogen atom of Val332 (H) and the carbonyl oxygen atom of Ile55 (L), the Nε2 of Gln331 (H) and the Oδ1 of Asn57 (L), and between the Ser337 Oγ (H) and the side chain Oδ1 of Asn57 (L). Furthermore, the side chains of Tyr78 (H) and Tyr98 (L) have an aromatic T-stacking interaction, and Met319 (H) is buried in a hydrophobic environment provided by Leu11, Pro12, and Val150 of the L subunit, as is Ile328 (H), which interacts with Phe105, Phe148, and Ile96 of the L subunit (Figure 3). Thus, both polar and hydrophobic interactions stabilize the association of the H and L subunits. The association of the H and L subunits is commonly observed; already in 1969 several tryptic peptides of a mushroom tyrosinase preparation were found[41] that now can be attributed to the L subunit (e.g., the amino acid composition of peptide V corresponds to residues 7−15 of the L subunit, that of peptide VI to residues 139−145, and that of peptide VII to the C-terminal residues 148−150[41]).

H Subunit Is the Tyrosinase Domain. The H subunit comprises residues 2−392 of PPO3. No density is visible for Met1 and most of Ser2 and for any residues beyond 392. It contains 13 α-helices, eight mostly short β-strands and many loops (Figure 1a). Its core structure is similar to the tyrosinase domain of *S. castaneoglobisporus* (*Sc*TYR; rmsd 1.7 Å, 211 matched residues), *Octopus dofleini* hemocyanin (rmsd 1.6 Å, 219 matched residues), *Bacillus megaterium* tyrosinase (*Bm*TYR; rmsd 1.6 Å, 193 matched residues), and *I. batatas* catechol oxidase (*Ib*COX; rmsd 1.6 Å, 189 matched residues). However, compared to the other type 3 copper proteins, *Ab*TYR is much larger, having about 100−120 more residues that are mostly present in loops connecting the secondary structure elements of the core domain (Supporting Information Figures S2 and S3).

A bundle of four helices (α3, α4, α10, and α11) in the center of the domain make up the catalytically essential binuclear copper-binding site (Figure 4a). The H subunit comprises the tyrosinase core region as defined by Flurkey and Inlow,[7] which starts at the conserved Arg20 and ends with Tyr365. The first residue of the core region, Arg20, is part of a short peptide stretch (residues 18−20), which lies parallel to residues 363−365. Arg20 stacks via a π-cation interaction with the Phe363 side chain in this latter stretch and is hydrogen-bonded to the conserved Glu102 (part of the Cu-A binding motif; see below) and Asp300 (part of the Cu-B binding motif). Phe363 is the first residue of a Tyr/Phe-X-Tyr conserved sequence motif, of which the tyrosine, Tyr365, is hydrogen-bonded to one of the side chain Nη's of Arg20. The equivalents to Arg20, Glu102, Asp300, and the Tyr/Phe-X-Tyr sequence motif are also present in *O. dofleini* hemocyanin, *Ib*COX, and *Sc*TYR, although in this latter protein the second aromatic residue is a Phe. These residues serve to stabilize the N- and C-terminal regions of the tyrosinase core domain as well as the Cu-A and Cu-B binding motifs.

The core region is followed by a 27-residue extension, containing a short 3_{10}-helix (residues 368−372) and α-helix α13 (residues 375−391) (Figure 1a). The extension ends with residues Tyr391-Gly392, which are conserved in fungal tyrosinases.[42,43] The hydroxyl group of Tyr391 has hydrogen-bonding interactions with the side chains of the functionally conserved Asp137 and Arg301, ensuring that the C-terminal end of the extension is closely associated with the tyrosinase core domain. No density is visible for Phe393 and beyond.

L Subunit Has a Lectin-like Fold. The L subunit comprises residues 9−28 and 35−150 of ORF 239342. No density is visible for the first 8 residues and residues 29−34 (Figure 4b). Likely, proteolytic cleavage has occurred between residues Leu31 and Ala32, since previously an N-terminal sequence of the L subunit was determined as ATNSGTLIIFDQ,[6] which corresponds to residues 32−43 of ORF 239342. It is not known which protease is responsible for the cleavage. The C-terminal residues Phe148-Ala149-Val150 are in agreement with a previous C-terminal sequence analysis.[41]

The L subunit adopts a β-trefoil fold, consisting of 12 antiparallel β-strands assembled in a cylindrical barrel of six 2-stranded sheets. A structural homologue search using DALI[44] revealed several homologues, covering mostly fibroblast growth factors and lectin-like proteins. The closest structural homologue was the hemagglutinating protein HA33 from *Clostridium botulinum*[45] with a *Z*-score of 16.7, an rmsd of 1.9 Å, and 14% sequence identity for 120 aligned residues. Other DALI matches included the ricin-B-like lectins, which, like HA33, are carbohydrate-binding proteins. Their carbohydrate-binding sites have been characterized, but the carbohydrate-binding residues are not conserved in the L subunit. Thus, a role of the L subunit in carbohydrate binding or cell wall attachment seems not likely.

A BLAST search[31] with ORF 239342 gave some hits of up to 26% identity with fragments of other larger proteins, but no

dx.doi.org/10.1021/bi200395t |*Biochemistry* 2011, 50, 5477–5486

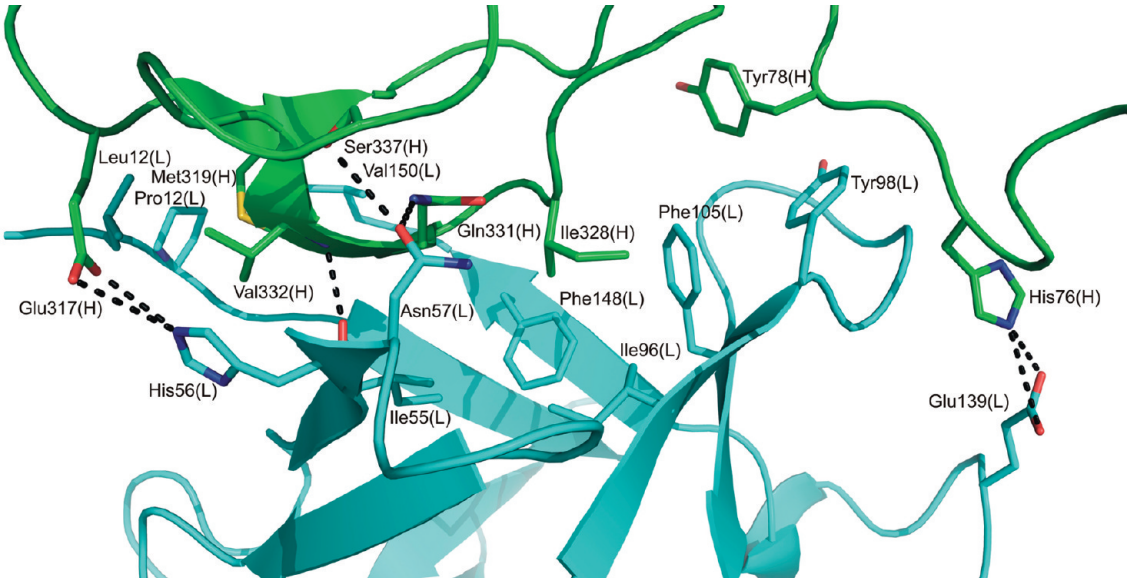

Figure 3. Atomic details of the interface between the H and L subunits of *A. bisporus* tyrosinase. The coloring of the peptide backbone is the same as in Figure 2. Amino acids in the interface are indicated in sticks and are colored according to atom type (green (H-subunit) or cyan (L-subunit) for carbon, and blue, red, yellow for nitrogen, oxygen, sulfur, respectively). Hydrogen-bonding interactions are shown as black dashed lines.

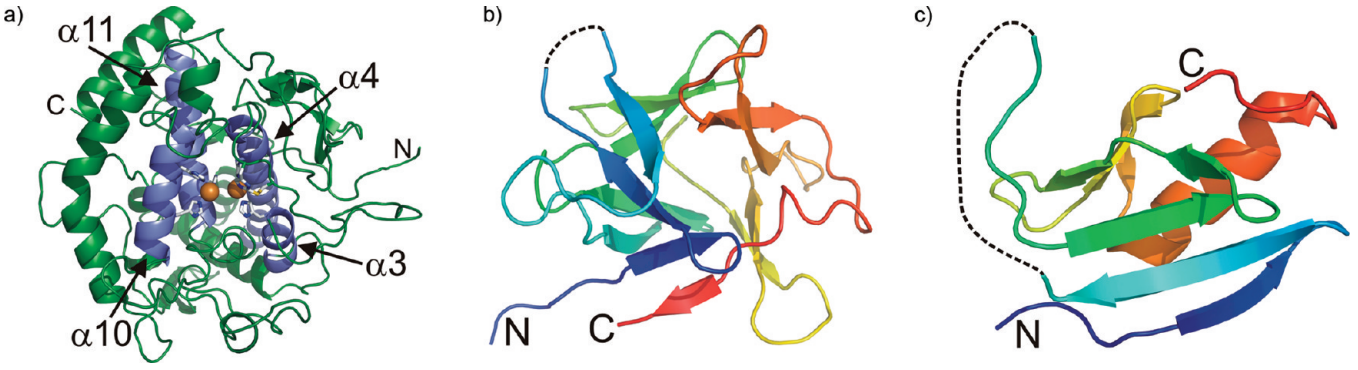

Figure 4. Cartoon representation of the individual subunits. (a) The H subunit (tyrosinase subunit), with the six copper-coordinating histidine residues and the cysteine colored to atom type. The thioether bond between Cys83 and His85 is indicated in yellow. The brown spheres are the Cu-A (right) and Cu-B (left). The backbone coloring is the same as in Figure 2. (b) The lectin-like subunit, in rainbow coloring from N- (blue) to C-terminus (red). The dashed line indicates the residues not visible in the electron density. (c) The caddie protein (ORF378) of the tyrosinase from *S. castaneoglobisporus*. The color coding is the same as in (b).

insights on the function of the L chain could be derived from this. For instance, residues 39−150 of the L chain show 26% identity (29 out of 112 residues) to residues of pantoate-β-alanine-ligase, but 22 out of 25 conserved residues that characterize the pantoate-β-alanine-ligase family are not present in the L chain, and the available pantoate−β-alanine−ligase 3D structures are all α-helical and do not resemble the β-trefoil fold of the L chain.[46]

Finally, the L subunit does not show any sequence or structural similarity to the caddie protein of *S. castaneoglobisporus* tyrosinase. The β-trefoil fold of the L subunit is completely different from the SH2-domain-like 6-stranded β-sheet + α-helix structure of the caddie protein (Figure 4b,c). The L subunit also binds to a very different region of the tyrosinase domain. While the caddie protein blocks the active site of *Sc*TYR, the *Ab*TYR L subunit is ∼25 Å away from the active site, and none of its residues hinders access to the active site. In addition, activity measurements in our lab resulted in specific activities of 752 kat/mol of enzyme for the H-only[5] and of 699 kat/mol for the H_2L_2 form of the enzyme.[6] From this we conclude that the L-chain does not exert a dramatic effect on the activity of the enzyme. However, as a caveat, the H-only tyrosinase was isolated from the natural complex, and involvement of the L subunit in H subunit folding, Cu binding, or stability *in vivo* cannot be excluded. Therefore, further research is needed to establish the biological role of the L subunit, if any, as well as its importance for the functioning of the H subunit.

Binuclear Copper Binding Site. The H subunit of *Ab*TYR contains a binuclear copper site, with each copper ion coordinated by three histidine residues. The site is located at the heart of two pairs of antiparallel α-helices (α3/α4 and α10/α11, respectively), which make an angle of nearly 90° with each other (Figure 4a). The ligands of the first copper ion, Cu-A, are the Nε2 atoms of His61 (end of helix α3), His85 (in the loop connecting α3 and α4), and His94 (beginning of α4). The second copper ion, Cu-B, has as ligands the Nε2 atoms of His259, His263 (α10), and His296 (α11). Viewed along the

dx.doi.org/10.1021/bi200395t |*Biochemistry* 2011, 50, 5477–5486

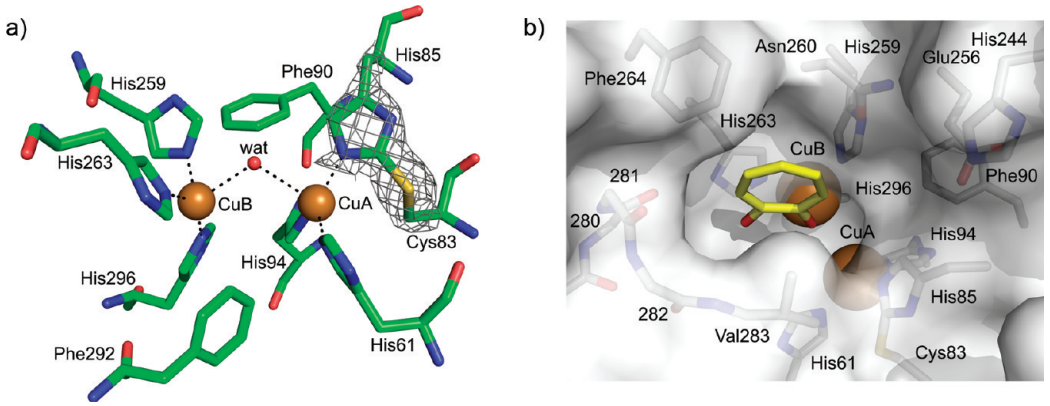

Figure 5. (a) Geometry of the binuclear copper-binding site in the orthorhombic space group. The ligands are colored according to atom type (green, blue, red, yellow for carbon, nitrogen, oxygen, sulfur, respectively). The brown spheres are the Cu-A and Cu-B copper ions, and the red sphere is a bound water molecule/hydroxyl ion. The electron density for the covalent thioether bond between the Cys83 Sγ and His85 Cε1 atoms is contoured at 2.0 σ and is shown in black mesh. (b) Geometry of the active site as surface representation with tropolone in sticks. Amino acids in the cavity are indicated in stick representation; for residues 280−282 only backbone sticks are shown.

Cu-A−Cu-B axis the histidine side chains are staggered, although His296 deviates somewhat (Figure 5a). Four of these histidine residues (61, 94, 259, 263) make hydrogen bonds from their Nδ1 atoms to a peptide carbonyl oxygen atom, which restricts their side chain rotational freedom and may contribute to the affinity for the metal. A covalent thioether bond with Cys83 fixes the orientation of the His85 side chain (Figure 5a). His296 is the only copper ligand of which the side chain has no direct interactions with other protein residues. However, its side chain is kept in position by a hydrogen bond to an internal water molecule, which, in turn, is hydrogen bonded to the carbonyl oxygen atom of His296 and another water molecule hydrogen bonded to Oδ1 of the conserved Asp300 and O of Pro91. Thus, the copper-coordinating histidine residues all have interactions that limit their rotational freedom. In addition, Phe90 is wedged between His94, His259, and His296, while Phe292 is between His61, His263, and His296, thereby also restricting the histidine side-chain conformations to maintain the integrity of the copper binding sites.[47] Phe90 and Phe292 are part of the highly conserved Phe-X_3-His motifs of tyrosinases, catechol oxidase, and hemocyanins, in which His94 and His296 are the most C-terminal histidine ligand of the Cu-A and Cu-B ions, respectively.[47] As a result of these interactions, the histidine residues are not very flexible, and the temperature factors of their side chains (~20.0 Å^2) are close to the average *B*-factor of the H chains (20.5 Å^2).

Geometry of the Binuclear Copper-Binding Site. Both copper binding sites adopt a nearly planar trigonal geometry. In agreement with density functional theory calculations,[48] the copper ions are slightly (0.5 ± 0.1 Å) out of the plane defined by the Nε2 atoms of their ligands. The distance between the Cu-A and Cu-B ions is 4.5 ± 0.2 Å, which is close to the 4.2 Å distance calculated for the deoxyhemocyanin binuclear copper site[48] and the 4.1, 4.5−4.9, and 4.4 Å distances observed in deoxy-*Sc*TYR,[9] *Manduca sexta* prophenoloxidase,[49] and *Ib*COX,[8] respectively. This suggests that the copper center in our *Ab*TYR structure is in the deoxy state.

A water molecule or hydroxyl ion bridges the two copper ions at distances of 2.65 ± 0.2 Å to Cu-A and Cu-B (Figure 5a; Figure S4 of the Supporting Information). It completes the four-coordinate trigonal pyramidal coordination sphere for both copper ions. The water molecule is nearest to the side chain of His259 (3.1 ± 0.1 Å from its Cε1 atom) but does not have hydrogen-bonding interactions with nitrogen or oxygen atoms of the protein. A single bridging water molecule has also been observed in the crystal structures of *S. castaneoglobisporus* deoxytyrosinase[9] and *M. sexta* prophenoloxidase.[49]

Substrate-Binding Site and Tropolone Binding. The binuclear copper-binding site is located at the bottom of a spacious cavity in the surface of the H subunit. This cavity is readily accessible from the solvent, and not occluded by the L subunit or by loops of side chains of the H subunit. The slow-binding, reversible tyrosinase inhibitor tropolone[50,51] binds in this cavity without the need for conformational changes of the protein (Figure 5b). It binds in a position somewhat similar to that of the phenylthiourea inhibitor of *Ib*COX[8] and of the tyrosine side chain of the caddie protein in the *Sc*TYR structure.[9] Its 7-membered aromatic ring is at van der Waals distance from the side chains of Val283 and the copper ligand His263 and has edge-to-face aromatic interactions with the side chain of Phe264. Details of the tropolone−protein binding interactions differ for the four molecules in the asymmetric unit, suggesting that tropolone is not bound very specifically. Its oxygen atoms have a shortest distance of about 3.0−3.5 Å to either Cu-A or Cu-B, depending on which of the four H subunits is considered. Since in the crystal structure of tropolone with a bound cupric ion the Cu−O distance is about 1.9 Å,[52] we conclude that the tropolone-binding mode represents a pre-Michaelis complex. This result is in agreement with the finding that tropolone only inhibits oxytyrosinase[51] and supports our conclusion that we have crystallized deoxytyrosinase. A similar unproductive binding mode has been observed for kojic acid bound to *Bacillus megaterium* tyrosinase.[53]

The active site is further lined with His244, part of the carboxylate of Glu256, Asn260, the main chain atoms of residues 279−282, and Ala286. Of these residues, His244, Glu256, and Ala286 are all conserved in PPO1, PPO2, PPO3, and PPO4 (Figure 1). Although they do not interact with the tropolone, they may interact with productively bound *bona fide* substrates. The space of the active site cavity is large enough to even accommodate phenolic steroids as substrates, as exemplified by the ability of the enzyme to *o*-hydroxylate compounds such as 17β-estradiol.[54]

Thioether Bond. In mushroom tyrosinase a thioether bond is formed post-translationally between the Cε atom of the Cu-A

ligand His85 and the side chain of Cys83. Clear electron density for the covalent bond is present, and both Cys83 and His85 are well-defined (Figure 5a). Binding of tropolone does not affect the residues. The role of the thioether bond in binuclear copper proteins is not clear. An essential, direct role in catalysis (by e.g. stabilizing the tyrosine radical generated during the reaction[55]) can be excluded because the thioether bond is not conserved.[8] Instead, it has been proposed that the thioether bond imposes structural restraints on the binuclear copper site to optimize its redox potential and allow rapid electron transfer.[8] However, in the absence of an oxytyrosinase structure and supporting quantum chemical evidence such a role remains speculative.

Implications for the Enzyme Reaction Mechanism. The precise reaction mechanism of tyrosinase is unclear. No information is available on the binding modes of the monophenolic substrate for the *o*-hydroxylation reaction and the diphenolic substrate for the oxidation reaction. On the basis of the structures of *Ib*COX and *Sc*TYR, it has been hypothesized that the monophenolic substrate is preoriented through a hydrophobic interaction with the Cu-B ligand His263 (PPO3 numbering).[10] Our PPO3-tropolone structure fully supports this notion. Next, the hydroxyl group of the substrate is proposed to be deprotonated by the peroxide ion bound between Cu-A and Cu-B at the start of the reaction. Whether the ensuing phenolate oxygen coordinates Cu-A or Cu-B is not clear at this moment.[9,10] Subsequently, an *ortho*-carbon atom of the substrate approaches the peroxide, and the substrate is *ortho*-hydroxylated. Although Matoba et al.[9] suggest that the *ortho*-hydroxylation would require the displacement of His54 (*Sc*TYR numbering), this seems improbable for *Ab*TYR since the equivalent His85 is covalently connected to Cys83 via a thioether bond and is therefore unlikely to move away. Finally, the diphenolic compound adduct undergoes oxidation to result in *o*-quinone product.[56]

Further details of the substrate binding mode and reaction mechanism may be obtained from detailed analysis of *Ab*TYR structures with bound substrates or substrate analogues in conjunction with spectroscopic analysis of crystals. Understanding of the interaction of tyrosinase with inhibitors may be of importance for evidence-based development of novel regulators of the enzyme's activity. Such compounds are actively searched for as a means to reduce the quality decay of food resulting from the action of oxidative enzymes.[57,58] The *Ab*TYR crystal structure may take this search from the ad-hoc nature that it has had until now to a more directed and targeted effort for this commercially important enzyme.

A. bisporus tyrosinase occurs in latent (inactive) and active forms. How the latent form is activated is not unequivocally known, although several hypotheses have been put forward, ranging from removal of active site-covering amino acids to removal of the entire C-terminal domain.[56,59,60] In all cases, improved substrate accessibility of the active site appears to be crucial. The current crystal structure suggests that the L subunit is not involved in the activation mechanism of mushroom tyrosinase, since it is located far away and not in a position to block access to the active site. A crystal structure of full-length mushroom tyrosinase may reveal whether the C-terminal part of the proenzyme that is cleaved off upon maturation plays a role in limiting access to the active site.

CONCLUSIONS

A commercially available tyrosinase from *A. bisporus* was crystallized and its structure was elucidated. The structure showed that the crystallized enzyme material consisted of PPO3. Six histidine residues coordinate the two copper ions in the active site with their Nε atoms. In turn, these histidine residues are held in place by hydrogen bonds of their Nδ atoms and by a thioether bond between Cys83 and His85. The ~4.5 Å distance between the two copper ions suggests that the enzyme is in the deoxy state. In the crystals an *A. bisporus* protein with a lectin-like fold was also present, but potential carbohydrate binding sites were not conserved. A complex with the inhibitor tropolone showed that tropolone binds in the active site but that it does not coordinate the copper ions, suggesting that it forms a pre-Michaelis complex.

ASSOCIATED CONTENT

Supporting Information. Additional figures showing the tetramers in space groups $P2_12_12$ and $P2_1$ (S1), a structure-based sequence alignment of tyrosinase-related type 3 copper proteins (S2), a superposition of the currently available tyrosinase crystal structures (S3, stereo), and the geometry of the binuclear copper-binding site (S4, stereo). This material is available free of charge via the Internet at http://pubs.acs.org.

AUTHOR INFORMATION

Corresponding Author

*Tel +31 (50) 3634381; Fax +31 (50) 3634800, e-mail b.w.dijkstra@rug.nl.

Author Contributions

⊥These authors contributed equally.

Funding Sources

This work was funded by the Innovation-driven Research Program for Industrial Proteins (project IIE00022). Data collection at the ESRF was supported by the ESRF and by the European Molecular Biology Laboratory (EMBL) under the European Community's Seventh Framework Program (FP7/2007−2013, grant agreement no. 226716).

ACKNOWLEDGMENT

We thank the Groningen Biomolecular Sciences and Biotechnology Institute (GBB) for providing the funding for the completion of the work and Prof. J. J. Beintema for his valuable advice and discussion.

ABBREVIATIONS

*Ab*TYR, *Agaricus bisporus* tyrosinase; *Bm*TYR, *Bacillus megaterium* tyrosinase; ESRF, European Synchrotron Radiation Facility; *Ib*COX, *Ipomoea batatas* catechol oxidase; NCS, noncrystallographic symmetry; PDB, Protein Data Bank; RACE, Rapid Amplification of cDNA Ends; *Sc*TYR, *Streptomyces castaneoglobisporus* tyrosinase; TLS, translation-libration-screw motion; tropolone, 2-hydroxy-2,4,6-cycloheptatrien-1-one.

REFERENCES

(1) Sanchez-Ferrer, A., Rodriguez-Lopez, J. N., Garcia-Canovas, F., and Garcia-Carmona, F. (1995) Tyrosinase: a comprehensive review of its mechanism. *Biochim. Biophys. Acta 1247*, 1–11.

(2) Wichers, H. J., Recourt, K., Hendriks, M., Ebbelaar, C. E. M., Biancone, G., Hoeberichts, F. A., Mooibroek, H., and Soler-Rivas, C.

(2003) Cloning, expression and characterisation of two tyrosinase cDNAs from *Agaricus bisporus*. *Appl. Microbiol. Biotechnol. 61*, 336–341.

(3) Wu, J., Chen, H., Gao, J., Liu, X., Cheng, W., and Ma, X. (2010) Cloning, characterization and expression of two new polyphenol oxidase cDNAs from *Agaricus bisporus*. *Biotechnol. Lett. 32*, 1439–1447.

(4) Strothkamp, K. G., Jolley, R. L., and Mason, H. S. (1976) Quarternary structure of mushroom tyrosinase. *Biochem. Biophys. Res. Commun. 70*, 519–524.

(5) Wichers, H. J., Gerritsen, Y. A. M., and Chapelon, C. G. J. (1996) Tyrosinase isoforms from the fruitbodies of *Agaricus bisporus*. *Phytochemistry 43*, 333–337.

(6) Schurink, M., van Berkel, W. J. H., Wichers, H. J., and Boeriu, C. G. (2007) Novel peptides with tyrosinase inhibitory activity. *Peptides 28*, 485–495.

(7) Flurkey, W. H., and Inlow, J. K. (2008) Proteolytic processing of polyphenol oxidase from plants and fungi. *J. Inorg. Biochem. 102*, 2160–2170.

(8) Klabunde, T., Eicken, C., Sacchettini, J. C., and Krebs, B. (1998) Crystal structure of a plant catechol oxidase containing a dicopper center. *Nat. Struct. Biol. 5*, 1084–1090.

(9) Matoba, Y., Kumagai, T., Yamamoto, A., Yoshitsu, H., and Sugiyama, M. (2006) Crystallographic evidence that the dinuclear copper center of tyrosinase is flexible during catalysis. *J. Biol. Chem. 281*, 8981–8990.

(10) Decker, H., Schweikardt, T., and Tuczek, F. (2006) The first crystal structure of tyrosinase: All questions answered? *Angew. Chem., Int. Ed. 45*, 4546–4550.

(11) Van Gelder, C. W. G., Flurkey, W. H., and Wichers, H. J. (1997) Sequence and structural features of plant and fungal tyrosinases. *Phytochemistry 45*, 1309–1323.

(12) Lerch, K. (1982) Primary structure of tyrosinase from *Neurospora crassa*. II. Complete amino acid sequence and chemical structure of a tripeptide containing an unusual thioether. *J. Biol. Chem. 257*, 6414–6419.

(13) Ismaya, W. T., Rozeboom, H. J., Schurink, M., Boeriu, C. G., Wichers, H., and Dijkstra, B. W. (2011) Crystallization and preliminary X-ray crystallographic analysis of mushroom *Agaricus bisporus* tyrosinase. *Acta Crystallogr. F67*, 575–578.

(14) Kabsch, W. (1993) Automatic processing of rotation diffraction data from crystals of initially unknown symmetry and cell constants. *J. Appl. Crystallogr. 26*, 795–800.

(15) Leslie, A. G. W. (2006) The integration of macromolecular diffraction data. *Acta Crystallogr. D62*, 48–57.

(16) Evans, P. (2006) Scaling and assessment of data quality. *Acta Crystallogr. D62*, 72–82.

(17) Collaborative Computational Project Number 4. (1994) The CCP4 suite: programs for protein crystallography, *Acta Crystallogr. D50*, 760−763.

(18) Matthews, B. W. (1968) Solvent content of protein crystals. *J. Mol. Biol. 33*, 491–497.

(19) Vagin, A., and Teplyakov, A. (1997) MOLREP: an automated program for molecular replacement. *J. Appl. Crystallogr. 30*, 1022–1025.

(20) The UniProt Consortium. (2007) The universal protein resource (UniProt), *Nucleic Acids Res. 35*, D193−D197.

(21) Saller, M. J., Fusetti, F., and Driessen, A. J. M. (2009) *Bacillus subtilis* SpoIIIJ and YqjG function in membrane protein biogenesis. *J. Bacteriol. 191*, 6749–6757.

(22) Jaroszewski, L., Rychlewski, L., Li, Z. W., Li, W. Z., and Godzik, A. (2005) FFAS03: a server for profile-profile sequence alignments. *Nucl. Acid Res. 33*, W284–W288.

(23) Cuff, M. E., Miller, K. I., van Holde, K. E., and Hendrickson, W. A. (1998) Crystal structure of a functional unit from *Octopus* hemocyanin. *J. Mol. Biol. 278*, 885–870.

(24) Perbandt, M., Guthöhrlein, E. W., Rypniewski, W., Idakieva, K., Stoeva, S., Voelter, W., Genov, N., and Betzel, C. (2003) The structure of a functional unit from the wall of a gastropod hemocyanin offers a possible mechanism for cooperativity. *Biochemistry 42*, 6341–6346.

(25) Canutescu, A. A., Shelenkov, A. A., and Dubrack, R. L. (2003) A graph theory for protein side-chain prediction. *Protein Sci. 12*, 2001–2014.

(26) McCoy, A. J., Grosse-Kunstleve, R. W., Storoni, L. C., and Read, R. J. (2005) Likelihood-enhanced fast translation functions. *Acta Crystallogr. D61*, 458–464.

(27) Terwilliger, T. C. (2003) Automated main-chain model building by template matching and interative fragment extension. *Acta Crystallogr. D59*, 38–44.

(28) Emsley, P., Lohkamp, B., Scott, W. G., and Cowtan, K. (2010) Features and development of Coot. *Acta Crystallogr. D66*, 486–501.

(29) Murshudov, G. N., Vagin, A. A., and Dodson, E. J. (1997) Refinement of macromolecular structures by the maximum-likelihood method. *Acta Crystallogr. D53*, 240–255.

(30) Lamzin, V. S., Perrakis, A., and Wilson, K. S. (2001) The ARP/wARP suite for automated construction and refinement of protein models in *International Tables for Crystallography* (Rossmann, M. G., Arnold, E., Eds.) pp 720−722, Kluwer Academic Publishers, Dordrecht, The Netherlands.

(31) Altschul, S. F., Gish, W., Miller, W., Myers, E. W., and Lipman, D. J. (1990) Basic local alignment search tool. *J. Mol. Biol. 215*, 403–410.

(32) Winn, M. D., Isupov, M. N., and Murshudov, G. N. (2001) Use of TLS parameters to model anisotropic displacements in macromolecular refinement. *Acta Crystallogr. D57*, 122–133.

(33) Lovell, S. C., Davis, I. W., Arendall, W. B., de Bakker, P. I. W., Word, J. M., Prisant, M. G., Richardson, J. S., and Richardson, D. C. (2003) Structure validation by C-alpha geometry: phi, psi, and C-beta deviation. *Proteins: Struct., Funct., Genet. 50*, 437–450.

(34) Schüttelkopf, A. W., and van Aalten, D. M. F. (2004) PRODRG: a tool for high-throughput crystallography of protein-ligand complexes. *Acta Crystallogr. D60*, 1355–1363.

(35) Shimanouchi, H., and Sasada, Y. (1973) Crystal and molecular structure of tropolone. *Acta Crystallogr. B29*, 81–90.

(36) Bond, C. S., and Schüttelkopf, A. W. (2009) ALINE: a WYSIWYG protein-sequence alignment editor for publication-quality alignments. *Acta Crystallogr. D65*, 510–512.

(37) Gouet, P., Robert, X., and Courcelle, E. (2003) ESPript/ENDscript: extracting and rendering sequence and 3D information from atomic structures of proteins. *Nucleic Acids Res. 31*, 3320–3323.

(38) DeLano, W. L. (2008) The PyMOL molecular graphics system, Delano Scientific LLC, Palo Alto, CA.

(39) Flurkey, A., Cooksey, J., Reddy, A., Spoonmore, K., Rescigno, A., Inlow, J., and Flurkey, W. H. (2008) Enzyme, protein, carbohydrate, and phenolic contaminants in commercial tyrosinase preparations: Potential problems affecting tyrosinase activity and inhibition studies. *J. Agric. Food Chem. 56*, 4760–4768.

(40) Jolley, R. L., Robb, D. A., and Mason, H. S. (1969) Multiple forms of mushroom tyrosinase - Association-dissociation phenomena. *J. Biol. Chem. 244*, 1593–1598.

(41) Jolley, R. L., Nelson, R. M., and Robb, D. A. (1969) Multiple forms of mushroom tyrosinase - Structural studies on isozymes. *J. Biol. Chem. 244*, 3251–3257.

(42) Marusek, C. M., Trobaugh, N. M., Flurkey, W. H., and Inlow, J. K. (2006) Comparative analysis of polyphenol oxidase from plant and fungal species. *J. Inorg. Biochem. 100*, 108–123.

(43) Kawamura-Konishi, Y., Tsuji, M., Hatana, S., Asanuma, M., Kakuta, D., Kawano, T., Mukouyama, E. B., Goto, H., and Suzuki, H. (2007) Purification, characterization, and molecular cloning of tyrosinase from *Pholiota nameko*. *Biosci. Biotechnol. Biochem. 71*, 1752–1760.

(44) Holm, L., Kaariainen, S., Rosenstrom, P., and Schenkel, A. (2008) Searching protein structure databases with DaliLite v.3. *Bioinformatics 24*, 2780–2781.

(45) Arndt, J. W., Gu, J., Jaroszewski, L., Schwarzenbacher, R., Hanson, M. A., Lebeda, F. J., and Stevens, R. C. (2005) The structure of the neurotoxin-associated protein HA33/A from *Clostridium botulinum* suggests a reoccurring β-trefoil fold in the progenitor toxin complex. *J. Mol. Biol. 346*, 1083–1093.

(46) Satoh, A., Konishi, S., Tamura, H., Stickland, H. G., Whitney, H. M., Smith, A. G., Matsumura, H., and Inoue, T. (2010) Substrate-induced closing of the active site revealed by the crystal structure of pantothenate synthetase from *Staphylococcus aureus*. *Biochemistry 49*, 6400–6410.

(47) Hazes, B., Magnus, K. A., Bonaventura, C., Bonaventura, J., Dauter, Z., Kalk, K. H., and Hol, W. G. J. (1993) Crystal structure of deoxygenated *Limulus polyphemus* subunit II haemocyanin at 2.18 Å resolution: clues for a mechanism for allosteric regulation. *Protein Sci. 2*, 597–619.

(48) Yoon, J., Fujii, S., and Solomon, E. I. (2009) Geometric and electronic structure differences between the type 3 copper sites of the multicopper oxidases and hemocyanin/tyrosinase. *Proc. Natl. Acad. Sci. U.S.A. 106*, 6585–6590.

(49) Li, Y. C., Wang, Y., Jiang, H. B., and Deng, J. P. (2009) Crystal structure of *Manduca sexta* prophenoloxidase provides insights into the mechanism of type 3 copper enzymes. *Proc. Natl. Acad. Sci. U.S.A. 106*, 17002–17006.

(50) Kahn, V., and Andrawis, A. (1985) Inhibition of mushroom tyrosinase by tropolone. *Phytochemistry 24*, 905–908.

(51) Espin, J. C., and Wichers, H. J. (1999) Slow-binding inhibition of mushroom (*Agaricus bisporus*) tyrosinase isoforms by tropolone. *J. Agric. Food Chem. 47*, 2638–2644.

(52) Macintyre, W. M., Robertson, J. M., and Zahrobski, R. F. (1966) Crystal structure of cupric tropolone - a refinement. *Proc. R. Soc. London, A 289*, 161–170.

(53) Sendovski, M., Kanteev, M., Shuster Ben-Yosef, V., Adir, N., and Fishman, A. (2011) First structures of an active bacterial tyrosinase reveal copper plasticity. *J. Mol. Biol. 405*, 227–237.

(54) Woerdenbag, H. J., Pras, N., Frijlink, H. W., Lerk, C. F., and Malingré, T. M. (1990) Cyclodextrin-facilitated bioconversion of 17-β-estradiol by a phenoloxidase from *Mucuna pruriens* cell cultures. *Phytochemistry 29*, 1551–1554.

(55) Ito, N., Phillips, S. E. V., Stevens, C., Ögel, Z. B., McPherson, M. J., Keen, J. N., Yadav, K. D. S., and Knowles, P. F. (1991) Nover thioether bond revealed by a 1.7 Å crystal structure of galactosidase. *Nature 350*, 87–90.

(56) Decker, H., Schweikardt, T., Nillius, D., Salzbrunn, U., Jaenicke, E., and Tuczek, F. (2007) Similar enzyme activation and catalysis in hemocyanins and tyrosinases. *Gene 398*, 183–191.

(57) Kim, Y.-J., and Uyama, H. (2005) Tyrosinase inhibitors from natural and synthetic sources: structure, inhibition mechanism and perspective for the future. *Cell. Mol. Life Sci. 62*, 1707–1723.

(58) Chang, T. S. (2009) An updated review of tyrosinase inhibitors. *Int. J. Mol. Sci. 10*, 2440–2475.

(59) Espin, J. C., van Leeuwen, J., and Wichers, H. J. (1999) Kinetic study of the activation process of a latent mushroom (*Agaricus bisporus*) tyrosinase by serine proteases. *J. Agric. Food Chem. 47*, 3509–3517.

(60) Espin, J. C., Soler-Rivas, C., and Wichers, H. J. (2000) Maturation and activation of latent tyrosinase from *Agaricus bisporus*. *Mushroom Sci. 15*, 79–86.